INTERNATIONAL JOURNAL FOR NUMERICAL METHODS IN FLUIDS
Int. J. Numer. Meth. Fluids 2000; **32**: 219–240

A numerical method for simulating discontinuous shallow flow over an infiltrating surface

Fritz R. Fiedler* and Jorge A. Ramirez

Colorado State University, Department of Civil Engineering, Fort Collins, CO 80523, USA

SUMMARY

A numerical method based on the MacCormack finite difference scheme is presented. The method was developed for simulating two-dimensional overland flow with spatially variable infiltration and microtopography using the hydrodynamic flow equations. The basic MacCormack scheme is enhanced by using the method of fractional steps to simplify application; treating the friction slope, a stiff source term, point-implicitly, plus, for numerical oscillation control and stability, upwinding the convective acceleration term. A higher-order smoothing operator is added to aid oscillation control when simulating flow over highly variable surfaces. Infiltration is simulated with the Green–Ampt model coupled to the surface water component in a manner that allows dynamic interaction. The developed method will also be useful for simulating irrigation, tidal flat and wetland circulation, and floods. Copyright © 2000 John Wiley & Sons, Ltd.

KEY WORDS: shallow water equations; finite difference; MacCormack scheme; upwind; point-implicit

1. INTRODUCTION

Hydrologists are often faced with the challenge of predicting the timing and magnitude of rainfall-generated run-off from watersheds for flood control, pollution prevention and ecological purposes. An important component of the rainfall run-off process is Hortonian overland flow, which is the shallow flow of water over the land surface prior to the major channelization that results when the rainfall rate exceeds the soil infiltration capacity in at least some areas of the watershed. In reality, the resulting overland flow depths and velocities are highly variable and discontinuous in space and time as a result of small-scale ground surface unevenness (microtopography) and natural spatial variation of soil hydraulic properties. In part, because of numerical difficulties associated with simulating this process, hydrologic modelers have traditionally been forced to simulate complex hillslopes as plane surfaces with constant hydraulic properties using simplified equations. Most often, the kinematic wave approximation to the full hydrodynamic equations is used. This approach, however, does not explicitly

* Correspondence to: Riverside Technology Inc., 2290 E. Prospect Road, Suite 1, Fort Collins, CO 80525, USA.

CCC 0271–2091/2000/020219–22$17.50

Received 30 October 1997
Revised 5 November 1998

account for microtopography and spatially variable soil properties, thus the small-scale dynamic interactions between surface and subsurface flow are ignored. The kinematic wave and infiltration model parameters are then simply fitting parameters, requiring calibration data, and physically based run-off predictions are accordingly difficult.

This paper presents a numerical method based on the MacCormack finite difference scheme developed for simulating two-dimensional, spatially variable overland flow at a small scale. The equations that describe this process are very similar to the well-known St. Venant and shallow water equations, thus, the developed numerical method or aspects thereof can be applied to a wide range of shallow water flow problems where discontinuous regimes are expected, such as irrigation, tidal flat circulation, flow in ephemeral stream channels, and flash floods.

2. EQUATIONS

The two-dimensional hydrodynamic overland flow equations can be derived from the Navier–Stokes equations by averaging over depth using kinematic boundary conditions and making certain assumptions, including: that velocity is constant with depth, the vertical velocity and acceleration components are small, the pressure distribution is hydrostatic, and horizontal shear stresses are small [1–3]. In terms of the dependent variables, depth, h, and unit discharge in the x- and y-directions, q_x and q_y respectively, these equations are

$$\frac{\partial h}{\partial t}+\frac{\partial q_x}{\partial y}+\frac{\partial q_y}{\partial y}-q_1=0, \tag{1}$$

$$\frac{\partial q_x}{\partial t}+\frac{\partial}{\partial x}\left(\frac{q_x^2}{h}+\frac{gh^2}{2}\right)+\frac{\partial}{\partial y}\left(\frac{q_x q_y}{h}\right)-gh(S_{0x}-S_{fx})=0, \tag{2}$$

$$\frac{\partial q_y}{\partial t}+\frac{\partial}{\partial y}\left(\frac{q_y^2}{h}+\frac{gh^2}{2}\right)+\frac{\partial}{\partial x}\left(\frac{q_x q_y}{h}\right)-(ghS_{0y}-S_{fy})=0, \tag{3}$$

where g is gravitational acceleration; the other terms in these equations are described subsequently.

Equation (1) results from conservation of mass over a control volume, and Equations (2) and (3) result from conservation of momentum in the x- and y-directions respectively. The source term q_1, lateral inflow, is the rate of water vertically added to or removed from the control volume. The various differential terms in the momentum equations represent different quantities related to conservation of momentum. In the x-direction, these terms are analogous to the terms in the classical St. Venant equations as follows:

$\frac{\partial q_x}{\partial t}$ local acceleration,

$\frac{\partial}{\partial x}\left(\frac{q_x^2}{h}\right), \frac{\partial}{\partial y}\left(\frac{q_x q_y}{h}\right)$ convective acceleration,

$\frac{\partial}{\partial x}\left(\frac{gh^2}{2}\right)$ pressure force.

The y-direction terms are related similarly.

The magnitude of q_1 at any point in space and time is determined from rainfall rates and infiltration characteristics; its computation is described later in Section 3.6. Interactive infiltration is a phrase sometimes used by hydrologists to refer to the dynamic interaction between surface flow and infiltration caused by spatially variable soil properties, microtopography, and/or rainfall. In essence, the amount of water available to interactively infiltrate at any point is the sum of the available rainfall, the depth of water at the point, and surface water flowing to that point from other areas (the dynamic component). Computation of this term depends on the infiltration model used to estimate point infiltration rates, and special treatment is required to ensure that fully interactive infiltration is simulated.

The bed slopes, S_{0x} and S_{0y}, are determined from the relative ground surface elevations, z, as

$$S_{0x} = -\frac{\partial z}{\partial x}, \qquad S_{0y} = -\frac{\partial z}{\partial y}. \tag{4}$$

Measured data are used to estimate these slopes in a manner that must be consistent with the numerical scheme.

Various methods exist for the evaluation of the friction slope terms, S_{fx} and $S_{fy.}$ The two-dimensional form of the Darcy–Weisbach (D–W) equation is primarily used to compute the friction slopes herein

$$S_{fx} = \frac{f}{8g}\frac{q_x(q_x^2+q_y^2)^{1/2}}{h^3}, \qquad S_{fy} = \frac{f}{8g}\frac{q_y(q_x^2+q_y^2)^{1/2}}{h^3}, \tag{5}$$

where f is the D–W friction factor. Natural overland flow is generally laminar, but is 'disturbed' by rainfall and topographic irregularities [4]. In the laminar flow regime, in which viscous stresses are much larger than Reynolds stresses, f is computed as a function of Reynolds number, Re, by the equation

$$f = \frac{K_0}{Re}, \tag{6}$$

where K_0 is a resistance parameter related to the ground surface characteristics [5]. The Reynolds number for two-dimensional flow is computed as

$$Re = \frac{(q_x^2+q_y^2)^{1/2}}{v}, \tag{7}$$

where v is the kinematic viscosity of water. After substitution, the laminar flow friction slope terms become

$$S_{fx} = \frac{K_0 v q_x}{8gh^3}, \qquad S_{fy} = \frac{K_0 v q_y}{8gh^3}. \tag{8}$$

To account for turbulent momentum transfer (Reynolds stresses), the well-known second-order turbulent viscosity terms

$$\varepsilon_l\left(\frac{\partial^2 q_x}{\partial x^2}+\frac{\partial^2 q_x}{\partial y}\right), \qquad \varepsilon_l\left(\frac{\partial^2 q_y}{\partial x^2}+\frac{\partial^2 q_y}{\partial y^2}\right) \tag{9}$$

can be added in the x- and y-directions respectively. In these terms, ε_l is the coefficient of turbulent viscosity or eddy coefficient [6].

To facilitate subsequent discussion of the numerical method, the overland flow equations are presented here in vector form

$$\frac{\partial \mathbf{U}}{\partial t}+\frac{\partial \mathbf{G}(\mathbf{U})}{\partial x}+\frac{\partial \mathbf{H}(\mathbf{U})}{\partial y}=\mathbf{S}(\mathbf{U}), \tag{10}$$

where

$$\mathbf{U}=[h,\, q_x,\, q_y]^T, \tag{10a}$$

$$\mathbf{G}(\mathbf{U})=\left[q_x,\, \frac{q_x^2}{h}+\frac{gh^2}{2},\, \frac{q_x q_y}{h}\right]^T, \tag{10b}$$

$$\mathbf{H}(\mathbf{U})=\left[q_y,\, \frac{q_y^2}{h}+\frac{gh^2}{2},\, \frac{q_x q_y}{h}\right]^T, \tag{10c}$$

$$\mathbf{S}(\mathbf{U})=\left[q_1,\, -gh\frac{\partial z}{\partial x}-\frac{K_0 v q_x}{8h^2}+\varepsilon_l\left(\frac{\partial^2 q_x}{\partial x^2}+\frac{\partial^2 q_y}{\partial y^2}\right),\, -gh\frac{\partial z}{\partial y}-\frac{K_0 v q_y}{8h^2}+\varepsilon_l\left(\frac{\partial^2 q_y}{\partial x^2}+\frac{\partial^2 q_y}{\partial y^2}\right)\right]^T. \tag{10d}$$

In these equations, T denotes the transpose, $\mathbf{G}(\mathbf{U})$ and $\mathbf{H}(\mathbf{U})$ are referred to as flux vectors, and $\mathbf{S}(\mathbf{U})$ as the source vector. Hereafter, these vectors will be shown as $\mathbf{G}$, $\mathbf{H}$ and $\mathbf{S}$, but the dependence on the vector of dependent variables $\mathbf{U}$ remains.

3. NUMERICAL METHOD

Several numerical challenges must be overcome before an adequate solution to these equations is obtained for discontinuous flow over an infiltrating surface. Zero depth is the true initial condition (before rainfall) at any point and persists until water ponds on the ground surface; some areas will not pond at all during a simulation. Numerically this is not allowed since depth appears in the denominator of several terms. As some areas are ponded and others not, the flow regime is discontinuous, and large gradients in the dependent variables occur. After ponding, the depths are generally small and correspondingly small numerical oscillations can destroy the solution. Given the oscillatory nature of the equations, oscillation control is a formidable challenge. Finally, the source terms are large compared with other terms in the equations and may vary greatly in time and space.

MacCormack's explicit predictor–corrector finite difference method [7] was chosen as the basic scheme after a review of the various numerical methods available [8]. This scheme has been successfully used to solve similar equations [2,9–11]. For the system of overland flow equations in two dimensions it is written

$$\mathbf{U}^*_{j,k} = \mathbf{U}^n_{j,k} - \frac{\Delta t}{\Delta x}(\mathbf{G}^n_{j,k} - \mathbf{G}^n_{j-1,k}) - \frac{\Delta t}{\Delta x}(\mathbf{H}^n_{j,k} - \mathbf{H}^n_{j,k-1}) + \Delta t\, \mathbf{S}^n_{j,k}, \tag{11a}$$

$$\mathbf{U}^{n+1}_{j,k} = 0.5\left[\mathbf{U}^n_{j,k} + \mathbf{U}^*_{j,k} - \frac{\Delta t}{\Delta x}(\mathbf{G}^*_{j+1} - \mathbf{G}^*_{j,k}) - \frac{\Delta t}{\Delta x}(\mathbf{H}^*_{j,k+1} - \mathbf{H}^*_{j,k}) + \Delta t\, \mathbf{S}^*_{j,k}\right]. \tag{11b}$$

The subscripts j and k are spatial indices in the x- and y-directions respectively, and the superscript n refers to the time level. The dependent variable vector predicted with Equation (11a), denoted with an *, is used to compute the differences in the corrector step (11b). As shown, backward spatial differences are used in the predictor step, and forward spatial differences in the corrector. In order to obtain second-order accuracy with the MacCormack scheme, it is necessary to alternate the spatial difference sequence in time. Here, for example, a forward–backward difference sequence would be used to compute $\mathbf{U}^{n+2}$. This form has been used previously for less spatially variable overland flow computations [2].

Appropriate initial and boundary conditions must be specified. For the desired simulation, the appropriate initial condition is zero depth and zero unit discharge everywhere in the domain. The best way to handle this initial condition is to assign small, insignificant starting depths [12]; the values used are discussed in subsequent paragraphs. In experimental plot overland flow simulations (rectangular plots), the subject of another aspect of this research for which this model was developed, closed boundaries formed by metal walls on three sides allow no through flow, so q_x and q_y perpendicular to these boundaries is set to zero. Depths at closed boundaries are determined by using inward differences in the continuity equation. At the plot outlet, an open boundary is simulated by using inward differences in both the continuity and momentum equations. Other boundary conditions are easily implemented for different applications.

The maximum time step (with respect to stability) allowable in the MacCormack scheme applied to linear hyperbolic equations is limited by the well-known Courant–Friedrich–Lewy (CFL) condition, as are all explicit finite difference methods. The overland flow equations are non-linear, however, and a rigorous stability analysis for these equations is exceedingly difficult. The source terms place additional and problem-dependent restrictions on the maximum admissible time step for stability. Therefore, the CFL condition can only be considered a general guideline here, and the maximum allowable time step for any particular problem will be less than predicted by the CFL condition and determined by numerical experimentation.

As noted, the MacCormack scheme in the form presented above has been applied to the overland flow equations [2]. While those authors attempted to simulate spatial variability similar in nature to what was desired for this research, several limitations of their model and thus the unmodified scheme are revealed upon close inspection. In order to circumvent the problem of zero depths, these authors appropriately used a finite minimum depth of water over the entire domain, but on the order of one-tenth the average steady state depth. Only fairly

large, positive lateral inflows were simulated at all nodes (approximately 150 mm h^{-1}, equivalent to an extremely large rainfall rate) starting at time zero, ensuring relatively large predicted flow depths at all times; a discontinuous flow regime was not simulated. Lateral inflow was constant in time, and interactive infiltration was not simulated. Finally, numerical oscillations were evident in most of the reported hydrographs produced with spatially variable source terms, and in the case of the single microtopographic surface modeled, apparently caused the simulation to abort at approximately 500 s [2]. These restrictions have been overcome with several modifications to the basic scheme.

3.1. Method of fractional steps

Two-dimensional finite difference schemes for systems of hyperbolic equations are sometimes split into a series of one-dimensional finite difference operators known as fractional steps [13]. A fractional step MacCormack scheme has been previously applied to the St. Venant equations and used to simulate reservoir and river flows [10]. In addition to simplifying application of the scheme to a two-dimensional problem, those authors found that larger time steps can be used. The fractional step MacCormack scheme is written

$$\mathbf{U}_{j,k}^{n+1} = L_x 2(\Delta t/2) L_y 2(\Delta/2) L_y 1(\Delta t/2) L_x 1(\Delta t/2) \mathbf{U}_{j,k}^{n}, \tag{12}$$

where L_x and L_y are one-dimensional difference operators, each applied twice and in a symmetrical manner. The first x-direction operator, $L_x 1$, is written

$$\mathbf{U}_{j,k}^{*} = \mathbf{U}_{j,k}^{n} - \frac{\Delta t}{2\,\Delta x}(\mathbf{G}_{j,k}^{n} - \mathbf{G}_{j-1,k}^{n}) + \frac{\Delta t}{2}\mathbf{S}_{x;\,j,k}^{n}, \tag{13a}$$

$$\mathbf{U}_{j,k}^{**} = 0.5\left[\mathbf{U}_{j,k}^{n} - \mathbf{U}_{j,k}^{*} - \frac{\Delta t}{2\,\Delta x}(\mathbf{G}_{j+1,k}^{*} - \mathbf{G}_{j,k}^{*}) + \frac{\Delta t}{2}\mathbf{S}_{x;\,j,k}^{*}\right]. \tag{13b}$$

Only the x-direction flux vector and source terms are used to compute the new values of the dependent variables, and the values computed in the corrector step are not representative of a particular time so they are denoted with **. The other operators have a similar form.

To retain second-order accuracy overall and not introduce any directional bias, a symmetric application of difference directions is required. Here, the following sequence was used:

$L_x 1$: Predictor, backward difference.
Corrector, forward difference.
$L_y 1$: Predictor, backward difference.
Corrector, forward difference.
$L_y 2$: Predictor, forward difference.
Corrector, backward difference.
$L_x 2$: Predictor, forward difference.
Corrector, backward difference.

Thus, a fractional step MacCormack scheme was applied to the overland flow equations, with second-order accuracy in both time and space.

3.2. Point-implicit friction slope treatment

The presence of depth in the denominator of several terms disallows zero depths, therefore, a finite minimum depth is assigned to each node that is not ponded. It is primarily the h^2 in the denominator of the friction slope term (after it is multiplied by gh) that limits the magnitude of the minimum depth. When depths are very small, the friction term is very large compared with the other terms in the momentum equations. As depths increase rapidly during the early stages of flow development, the friction slope term magnitude changes much faster than the other terms. This phenomenon renders the momentum equations stiff and severely limits the maximum admissible time step for stability; in fact, this phenomenon likely forced previous researchers to use very small time steps relative to their grid spacing (Courant numbers $\ll 1$) and keep lateral inflows and initial depths large [2]. One way to handle stiff differential equations is to use fully implicit methods. Alternatively, the offending source term(s) can be isolated and evaluated point-implicitly [14]. In the x-direction, the friction slope can be isolated and treated implicitly utilizing a Taylor series expansion about the nth time level at every point (j, k) in the domain

$$S_{fx}^{n+1} = S_{fx}^{n} + \left(\frac{\partial S_{fx}}{\partial q_x}\right)^{n} \Delta q_x + O(\Delta q_x^2), \tag{14}$$

where $\Delta q_x = q_x^{n-1} - q_x^n$. The partial derivative of the friction slope term with respect to q_x is easily obtained, and the second- and higher-order terms are dropped. The empirical friction slope term will likely contribute the largest error in Equations (10) [15]. Moreover, the coefficient f is generally unknown and determined by model calibration. Given the uncertainty associated with computation of the friction slope, ignoring the second-order terms in the above approximation will have little consequence, particularly in light of the benefits of point-implicit treatment.

Since Δq_x appears in the x-direction momentum difference equations, with some algebraic manipulations a scalar factor can easily be determined and inserted into the momentum equations to achieve the desired point-implicit treatment of the friction slope while maintaining the overall explicit character of the scheme. This factor is

$$D_x = \frac{1}{1 - \Delta t(\partial S_{fx}/\partial q_x)} \tag{15}$$

and is inserted, for example, into the L_x1 predictor step as

$$\mathbf{U}_{j,k}^{*} = \mathbf{U}_{j,k}^{n} - D\frac{\Delta t}{2\,\Delta x}(\mathbf{G}_{j,k}^{n} - \mathbf{G}_{j-1,k}^{n}) + D\frac{\Delta t}{2}\mathbf{S}_{x;\,j,k}^{n}, \tag{16}$$

where $D = 1$ when computing h and q_y, and $D = D_x$ when computing q_x. The point-implicit factor is derived and used similarly in the y-direction operators.

This method allows minimum depths on the order of 10^{-10} m or smaller to be used, many orders of magnitude less than steady state flow depths and clearly insignificant, and the time step restriction imposed by friction slope stiffness is removed. Flow depths are not allowed to be less than the minimum depth in the developed model, and q_x and q_y are also assigned minimum values, where h is minimum such that h is 5% greater than the critical depth (e.g. $h = 1.33 \times 10^{-11}$ m, $q_x = q_y = 1.00 \times 10^{-14}$ m s^{-1}).

3.3. Convective acceleration upwinding

Hyperbolic equations are oscillatory in nature, and the overland flow equations are no exception. The shallow water equations are known to be prone to high frequency or '$2\,\Delta x$' oscillations (oscillation wavelengths equal $2\,\Delta x$) when centrally differenced because the value of the slope estimated by the difference is independent of the value of the dependent variable at the mid-point [16]. Upwind methods can reduce these oscillations, but they are generally only first-order accurate. They are effective at reducing oscillations because disturbances in the flow regime that affect convective acceleration can not be propagated upstream. For the convection–diffusion equation, upwinding of the convective term has been shown to be effective for reducing $2\,\Delta x$ oscillations but the artificial diffusion introduced leads to low accuracy for diffusion [17]. Upwinding the full shallow water equations for marine-type applications has been reported to be inaccurate [3]. However, this study found that upwinding just the convective acceleration term within the MacCormack scheme reduces $2\,\Delta x$ oscillations tremendously while having little effect on the overall accuracy. The convective acceleration time discretization remains second-order accurate. To the knowledge of the authors, upwinding this term within the MacCormack scheme is unique to this model.

For example, in the predictor step of the backward-difference $L_x 1$ operator, for flow in the negative x-direction (from $j+1$ to j), the upwinded convective acceleration term is differenced

$$\frac{p^{n2}_{j+1,k}}{h^{n}_{j+1,k}} - \frac{p^{n2}_{j,k}}{h^{n}_{j,k}} \tag{17}$$

and thus a forward difference is used in both the predictor and corrector step. In this model, the type of difference used at each computational node is not allowed to change within an operator cycle. Also, the appropriate predictor–corrector difference sequence is applied conventionally in regions of converging flow, where second-order spatial accuracy is warranted, as well as adjacent to boundaries for consistency with the boundary conditions.

3.4. Numerical oscillation control

Numerical tests indicated that additional oscillation control is sometimes necessary for simulation of overland flow over surfaces with extreme hydraulic conductivity and microtopographic spatial variations. A method developed for the Euler equations [18] and used for computation of unsteady free-surface flows with shocks using explicit schemes [19] was implemented in the model after testing various forms of smoothing. This smoothing function

(also referred to as an artificial viscosity [19]) is particularly effective at controlling $2\Delta x$ oscillations. In the x-direction, the smoothing parameter is computed using the corrected values of depth, assumed here to be positive

$$\xi_{j,k} = \frac{\Delta x}{\Delta t} \frac{|h^{**}_{j+1,k} - 2h^{**}_{j,k} + h^{**}_{j-1,k}|}{h^{**}_{j+1,k} + 2h^{**}_{j,k} + h^{**}_{j-1,k}}, \tag{18a}$$

$$\xi_{j+1/2,k} = \varepsilon_2 \max(\xi_{j+1,k}\ \xi_{j,k}), \tag{18b}$$

where ε_2 is a coefficient used to control the amount of smoothing; reported typical values are in the range 0.5–3 [19], although much smaller values were used. The values of depth from the corrector step are then modified by

$$h^{***}_{j,k} = h^{**}_{j,k} + \xi_{j+1/2,k}(h^{**}_{j+1.k} - h^{**}_{j,k}) - \xi_{j-1/2,k}(h^{**}_{j,k} - h^{**}_{j-1,k}). \tag{19}$$

This procedure is performed after the application of each difference operator, in the appropriate direction. Addition of this smoothing function does not change the overall accuracy of the MacCormack scheme [19].

3.5. Bed slope and turbulent viscosity term

To determine the bed slopes of Equation (4) when using the MacCormack scheme, it is imperative to difference the input elevations (z) in the same direction as the depths are differenced in the pressure force terms of the momentum equations, particularly when the bed slopes change in space, to ensure a proper balance between these two terms. The bed slopes are multiplied by depth, and the arithmetic average depth computed in the direction of the difference should be used. For example, if a backward difference in the x-direction is used for the pressure force and bed slope terms, the bed slope is multiplied by the average depth $(h_{j-1,k} + h_{j,k})/2$. Finally, viscosity related to turbulent momentum exchange modeled by the second-order terms in Equation (9) is computed using standard central differences using the latest values of the dependent variables.

3.6. Lateral inflow and interactive infiltration

The occurrence of Hortonian overland flow is completely determined by rainfall and ground surface infiltration characteristics. A goal of this study was to account for fully interactive infiltration when computing lateral inflow rates such that the effects of the relationship between microtopography and infiltration characteristics on run-off could be explored. Therefore, rainfall was considered constant in time when applied, and a common infiltration model was used; it is the dynamic interaction allowed between surface water and infiltration due to spatial variations in infiltration parameters and microtopography that is unique in this model, not the infiltration model itself.

Saturation excess (Dunne) run-off generation is another important hydrologic mechanism related to overland flow, in which the soil surface becomes saturated from below (e.g. due to rising groundwater), thus precluding infiltration. For example, overland flow is often generated

in riparian areas due to shallow water tables. Incorporation of this mechanism was beyond the scope of this research. However, there are no limitations to the surface water component of the developed model which would disallow future incorporation of saturation excess runoff generation by adding additional methods for computing lateral inflow.

Currently, every node is considered to be initially not ponded (no surface water, but with the soil at a specified initial moisture content), and the infiltration capacity is greater than the rate of water supplied. The infiltration capacity at every computational node prior to ponding is determined by the well-known Green–Ampt infiltration model [20]

$$f_{cj,k} = K_{j,k}\left[\frac{\Psi_{j,k}\,\Delta\theta_{j,k}}{F_{j,k}} + 1\right], \tag{20}$$

where K is the effective hydraulic conductivity, Ψ is the wetting front suction, $\Delta\theta$ is the volumetric moisture content deficit (capacity minus initial) at the wetting front, and F is the cumulative depth of water infiltrated. The rate of water available to infiltrate is equal to the rainfall rate, r, plus any flow onto the node from adjacent nodes

$$i_{aj,k} = r + \frac{q^n_{x\ \mathrm{on}}}{\Delta x} + \frac{q^n_{y\ \mathrm{on}}}{\Delta x}, \tag{21}$$

where $q_{x\ \mathrm{on}}$ and $q_{y\ \mathrm{on}}$ are determined by summing the adjacent-node discharges that are in the direction of node (j, k). In this manner, overland flow generated in one area is allowed to infiltrate into other areas if the capacity exists at any time in the simulation; thus, fully interactive infiltration is simulated. If the node remains unponded ($f_c \geq i_a$), then the average infiltration rate over the time step is determined

$$f^{\mathrm{ave}}_{j,k} = i_{aj,k}. \tag{22}$$

Ponding is also allowed to occur within a time step using a simple, well-known procedure [21], even though the time steps normally used in these simulations are very small and the error associated with not allowing for this phenomenon is likely negligible.

If a node is ponded ($f_c < i_a$), the rate available to infiltrate includes the depth of water on that node

$$i_{aj,k} = r + \frac{h^n_{j,k}}{\Delta t} + \frac{q^n_{x\ \mathrm{on}}}{\Delta x} + \frac{q^n_{y\ \mathrm{on}}}{\Delta y}. \tag{23}$$

If this rate is greater than the infiltration capacity, F^{n+1} is computed using the Green–Ampt equation for cumulative infiltration

$$F^{n+1}_{j,k} - F^n_{j,k} - \Psi_{j,k}\ln\left[\frac{F^{n+1}_{j,k} + \Psi_{j,k}\Delta\theta_{j,k}}{F^n_{j,k} + \Psi_{j,k}\Delta\theta_{j,k}}\right] = K_{j,k}\Delta t, \tag{24}$$

which is solved using the well-known Newton–Raphson method [22]. The average infiltration rate over the time interval is then estimated

$$f_{j,k}^{\text{ave}} = \frac{F_{j,k}^{n+1} - F_{j,k}^{n}}{\Delta t}. \tag{25}$$

In both cases, the average lateral inflow rate at a point over the time step is computed as the difference between the rainfall rate and the infiltration rate

$$q_{\text{l}j,k} = r - f_{j,k}^{\text{ave}} \tag{26}$$

and is held constant over each time step. This source term does not act in either the x- or y-direction (q_{l} is assumed to be added to the control volume vertically), so half the computed value is applied in the x-direction fractional steps, and half in the y-direction.

As defined here, lateral inflow at any particular node (j, k) can vary from a minimum value equal to

$$q_{\text{lmin}} = -\left[\frac{h}{\Delta t} + \frac{q_{x\ \text{on}}}{\Delta x} + \frac{q_{y\ \text{on}}}{\Delta y}\right], \tag{27}$$

where all surface water on the node and coming towards the node from adjacent nodes is infiltrated, to a maximum value of

$$q_{\text{lmax}} = r, \tag{28}$$

which is the case for rainfall on an impervious surface. Typically, lateral inflow varies from 0 to r in rainfall excess-type hydrologic models, although minimum values equal to $-h/\Delta t$ occur in models that allow partial interaction, i.e. only after rainfall [23].

4. RESULTS AND DISCUSSION

4.1. Comparative examples

The general properties of the basic MacCormack scheme and numerous numerical tests of it related to similar equation sets have been reported elsewhere [2,7,9–11,19,24]. Here this paper presents the results of several numerical comparisons performed to show the developed model's effectiveness related to spatially variable overland flow. Four comparisons are made: (1) steady state results are compared with the kinematic wave solution for a plane with constant lateral inflow, (2) a comparison is made with an analytical solution of a dam break problem, (3) model results are compared with results of an experiment where spatially variable lateral inflow was applied to a three-plane cascade, and (4) outflow hydrographs are computed and compared with some recently published results for overland flow on an infiltrating plane. The first comparative example is used as a general indicator of the ability of the hydrodynamic

model to predict the flow variables for a simple case; large differences would indicate mass balance problems. The second and third examples are more rigorous tests of the surface water component of the model and its shock capturing ability. The fourth example tests both the model's infiltration and surface water components.

Table I shows the input parameters for the first comparative example. Model results for this example were computed with a constant D–W friction factor, 20 grid points with $\Delta x = 1.60421$ m, $\Delta t = 0.5$ s, and are shown in Table II. There is less than 1% difference between depth and discharge computed by the models at the end of the plane.

The one-dimensional dam break problem comprising the second comparative has been previously reported [25]. In this problem, a shock wave develops due to the instantaneous break of a 'dam' at $x = 1000$ m, with the height of water on one side equal to 10 m, and the height of water on the other side equal to 5 m. The channel bed is assumed to be horizontal and frictionless. Figure 1 shows the model results compared with the analytical solution at 50 s produced with $\Delta x = 5$ m and $\Delta t = 0.8333$ s. For this problem $\varepsilon_1 = \varepsilon_2 = 0$. It is interesting to note here that upwinding the convective acceleration term does not appear to affect the model accuracy or ability to capture shocks in a problem where this term plays a relatively large role.

Results from rainfall run-off experimental simulations on a 24 m long cascade of three aluminum planes with spatially variable lateral inflow configured such that shocks form [26] are compared with model results in the third example. Each plane section was 8 m long, with slopes of 0.02, 0.015 and 0.01 in the downstream direction. In the most difficult scenario to simulate, each section received constant lateral inflows of 389, 230 and 288 cm h^{-1} respectively, for a duration of 10 s. Figure 2 shows the model-predicted outflow hydrograph compared with the experimental results produced with $\Delta x = 0.25$ m and $\Delta t = 0.05$ s. In this experiment, a shock wave is produced, which arrives at the downstream end of the cascade at approximately 25 s; the developed model reproduces these results well considering the potential experimental errors, such as non-uniform lateral inflow [25], and better than other published analytical and numerical methods [2,26,27]. Here, Manning's equation was used to compute friction slope, with a friction coefficient of 0.009.

Table I. Input parameters for the steady state kinematic wave test

Lateral Inflow	25.4 mm h^{-1}
Length of plane	30.48 m
Bed slope	0.05
D–W friction factor	0.265

Table II. Results for the steady state kinematic wave test

	Depth (cm)	Discharge (cm^2 s^{-1})
Kinematic wave	0.1462	2.1505
Hydrodynamic model	0.1471	2.1418
Percent difference	0.62	0.40

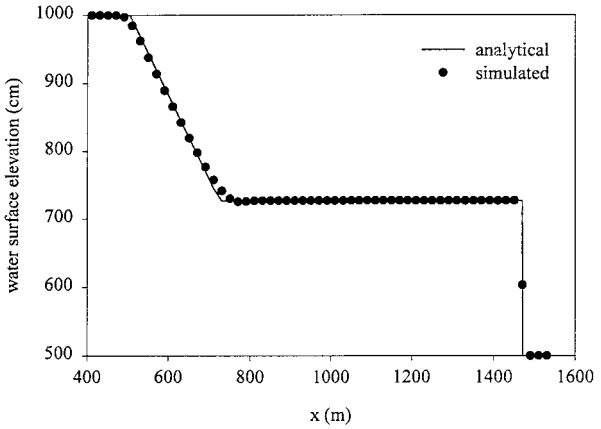

Figure 1. Results for the dam break problem.

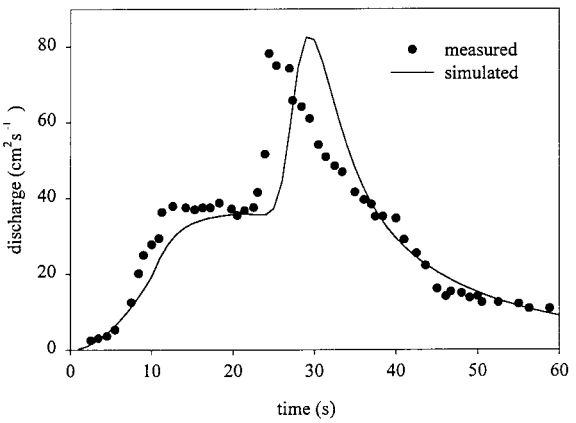

Figure 2. Measured and simulated results for Iwagaki's [26] experiment.

The fourth comparison uses some recently published results of overland flow simulations on a 50 m long plane with spatially variable infiltration parameters [23]. Their model is comprised of the kinematic wave equations coupled to the Smith–Parlange infiltration equation [28] solved with a finite difference scheme on a characteristic computational net. There are several important differences between their model and the current model that must be described before the comparison is made.

A different infiltration model was used to compute lateral inflow; however, proper choice of the Green–Ampt parameters Ψ and $\Delta\theta$ corresponding to the Smith–Parlange parameter B will cause the models to yield almost identical results. These near-equivalent parameters are derived using the approximation of Youngs for the soil sorptivity, S [29]

$$S = \sqrt{2\Delta\theta K\Psi}, \tag{29}$$

and the relationship between the Smith–Parlange infiltration model parameters B and S [28]

$$B = \frac{S^2}{2K}. \tag{30}$$

Combining these equations results in $B = \Psi\Delta\theta$. In this case, $B = 11$ cm, for which $\Psi = 44$ cm and $\Delta\theta = 0.25$ were chosen (note that other $\Psi - \Delta\theta$ pairs could also be used). A comparison of these models reveals that the Green–Ampt model predicts a slightly higher infiltration capacity (and less rainfall excess) than the Smith–Parlange model as a function of cumulative infiltration. Figure 3 shows infiltration capacity as a function of cumulative infiltration for the near-equivalent parameter values stated above, and a hydraulic conductivity value of 3.53×10^{-4} cm s^{-1}. When cumulative infiltration is zero, the curves converge, and as cumulative infiltration increases they diverge and become essentially parallel. In light of these results, the discharge predicted with the hydrodynamic model is expected to be slightly less than that predicted with the kinematic wave model.

Manning's equation was used for the friction slope term [23]; for this comparison the developed hydrodynamic code was modified to use Manning's equation as well. The following simulations were performed using $\Delta x = 0.25$ m and $\Delta t = 0.1$ s.

Three cases with different deterministic hydraulic conductivity variations are presented here: (1) constant hydraulic conductivity over the plane, (2) hydraulic conductivity decreasing linearly with distance in the downslope direction, and (3) hydraulic conductivity increasing linearly with distance in the downslope direction. In all cases, the mean value of hydraulic conductivity is the same, equal to 3.53×10^{-4} cm s^{-1}. The minimum and maximum values

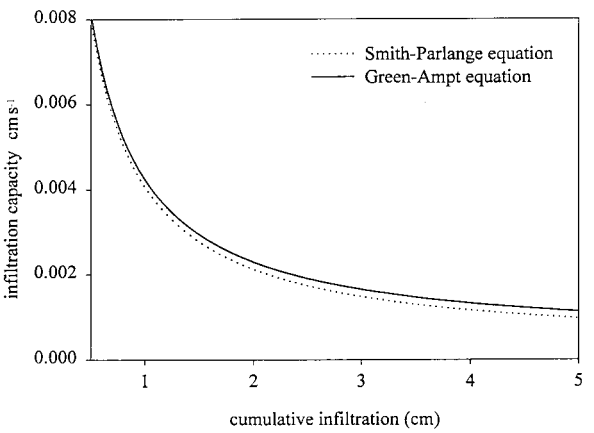

Figure 3. Infiltration capacity curves for the Green–Ampt and Smith–Parlange infiltration capacity curves with near-equivalent parameters.

were 2.37×10^{-4} and 4.70×10^{-4} cm s^{-1} respectively. Other model parameters are presented in Table III.

Figures 4–6 show the results of both models for cases (1), (2) and (3) respectively. It is seen from these figures that the hydrodynamic model results are very close to those produced with a characteristic-based kinematic solution on a plane where the kinematic approximation

Table III. Input parameters for the infiltrating kinematic wave test

Rainfall rate	177.6 mm h^{-1}
Rainfall duration	20 min
Length of plane	50 m
Bed slope	0.04
Manning's n	0.1

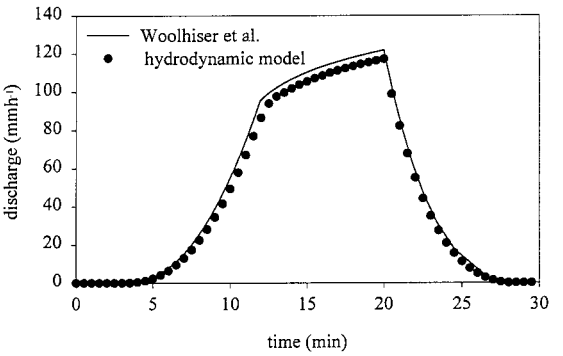

Figure 4. Results for an infiltrating plane, uniform K (case (1)).

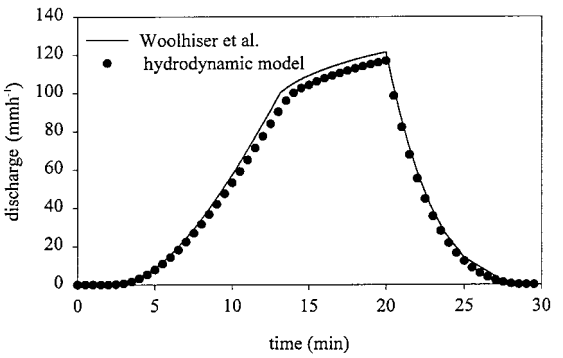

Figure 5. Results for an infiltrating plane, K decreasing downslope (case (2)).

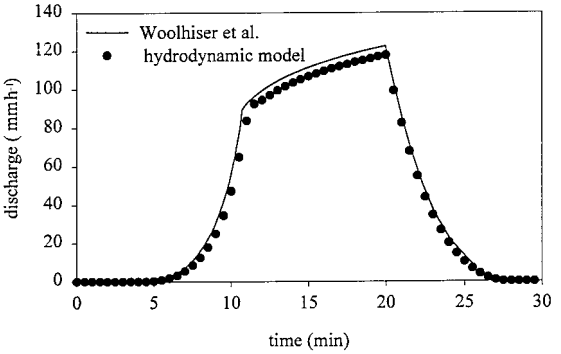

Figure 6. Results for an infiltrating plane, K increasing downslope (case (3)).

should be close to the solution of the full hydrodynamic equations, and the difference is attributable to the different infiltration models.

4.2. Applications

The mathematical model presented in this paper was developed to explore the effects of spatially variable infiltration and microtopography on overland flow. Data to support such simulations were collected from a semi-arid grassland in northeastern Colorado. Here, we were also interested in the potential effects of grazing on hydrologic response with respect to spatially variable hydrodynamics and interactive infiltration. The results of a few simulations are presented below that show the utility of the developed model in this respect.

The bottom portion of Figure 7 is a ground surface plot, developed using measured microtopographic relief data [8], of an approximately 1 m^2 area of grassland. The top portion of this figure shows the predicted flow depths after 25 min of simulated rainfall at 58.4 mm h^{-1}. This simulation was performed with the spatially constant infiltration parameters: $K = 2.1 \times 10^{-4}$ cm s^{-1}, $\Psi = 11$ cm and $\Delta\theta = 038$. The resistance parameter K_0 was assumed to be 1500, in the range reported for sparse vegetation [5]. The domain was discretized with a constant grid spacing of 1 cm in both the x- and y-directions and a time step of 0.025 s. The coefficient of turbulent viscosity, ε_1, was assumed to be equal to 2.0, and the smoothing parameter, ε_2, was 0.002. Figure 8 shows the model-predicted velocity vectors for the same time. The hydrodynamic model predicts the complex, spatially variable flow hydraulics associated with true overland flow. Even within this small area, there are regions of converging and diverging flow, and well-defined microchannels (small, well-defined tortuous flow paths around microtopographic highs).

There is a particular relationship between vegetation and microtopography common on grasslands in semi-arid environments, where microtopographic lows (depressions) are occupied by bare soil, and highs (hummocks) by vegetated soil. The bare- and vegetated-soil patch size and microtopographic wavelength both range from approximately 0.05 to 0.5 m. Since the measured bare-soil hydraulic conductivity is about an order of magnitude less than the

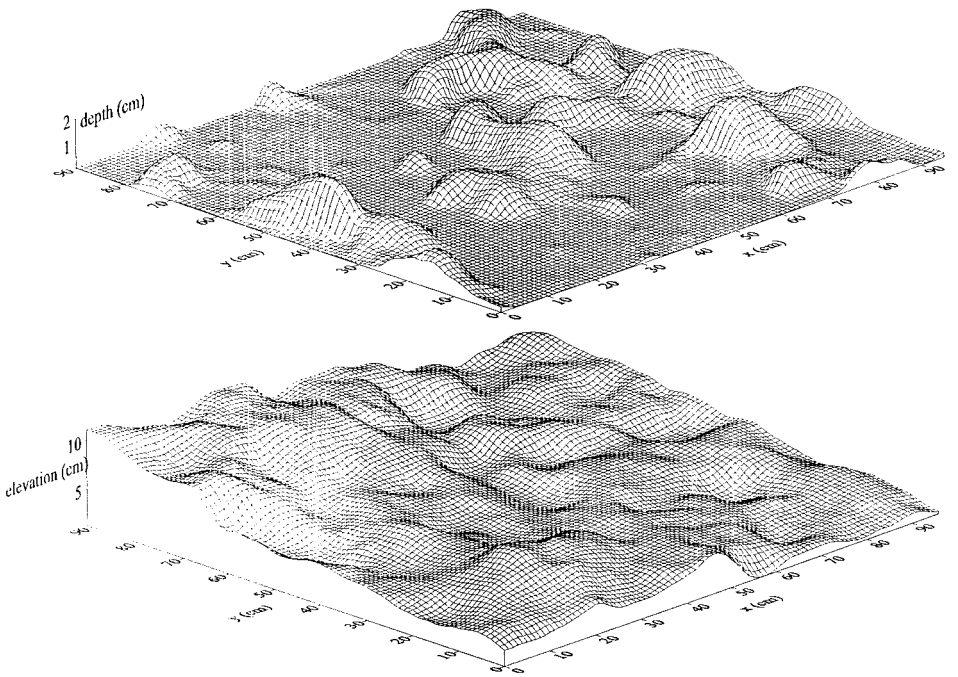

Figure 7. Microtopographic ground surface and predicted flow depths for first example application.

measured vegetated-soil conductivity, rainfall will cause water to pond on bare soil well before on vegetated soil. Bare-soil water depths increase as a rainfall event progresses, and vegetated zones become inundated as water migrates on the ground surface and ground-surface depressions fill. Since the hydraulic conductivity, and therefore infiltration capacity of the vegetated soil, is large, water that ponds in bare areas can infiltrate into vegetated areas as they become inundated. This aspect of interactive infiltration (run-on at a small scale), not accounted for by other rainfall run-off models, has a significant effect on the hydrologic response of grasslands [8].

A spatial distribution of infiltration parameters that mimics the physical system can be developed from the microtopographic data presented in Figure 7 by assigning all nodes with elevations greater than the mean elevation infiltration parameters representative of vegetated soil, and assigning all nodes with elevations less than the mean elevation infiltration parameters representative of bare soil. This distribution is shown on Figure 9 for the small area described previously. A simulation was performed with the bare-soil parameters $K = 2.1 \times 10^{-4}$ cm s^{-1}, $\Psi = 11$ cm and $\Delta\theta = 0.38$, and the vegetated-soil parameters $K = 1.5 \times 10^{-3}$ cm s^{-1}, $\Psi = 9$ cm and $\Delta\theta = 0.42$; these parameters were derived from field measurements and values typical of the observed soil types.

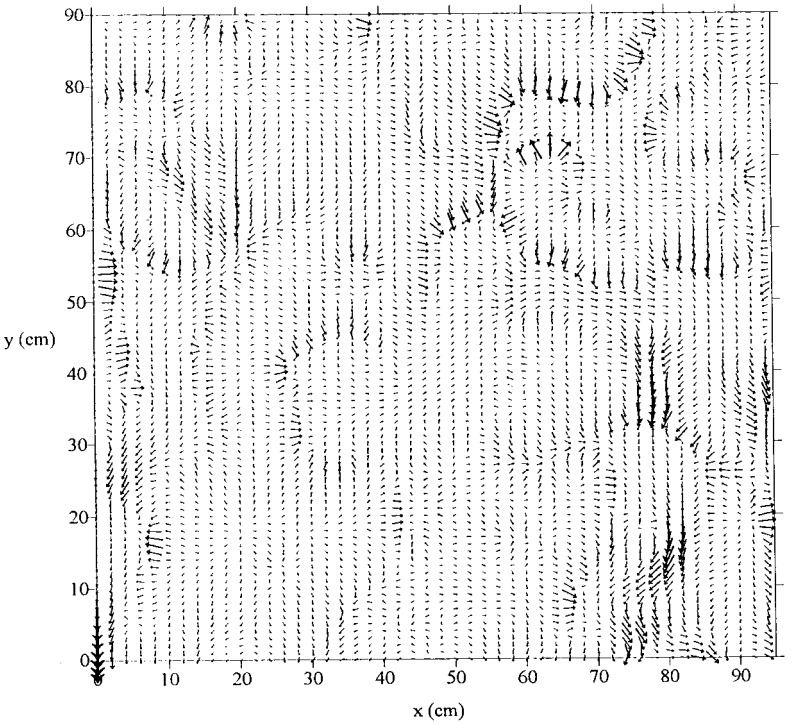

Figure 8. Velocity vectors of flow on the ground surface depicted on Figure 7. Maximum velocity is 7.43 cm s^{-1}.

With all other parameters the same as in the first example application, simulations were performed that illustrate the model's ability to simulate interactive infiltration. Figure 10 shows contours of the cumulative depth of infiltrated water. As expected, infiltrated depths are significantly greater at the bare/vegetated soil interfaces. Figure 11 shows the outflow hydrograph for this simulation, plus the outflow hydrograph for a simulation performed with a slightly increased vegetated-soil hydraulic conductivity. The decrease in observed run-off is solely attributed to interactive infiltration, since the simulated rainfall rate alone will not cause ponding on the vegetated soil at any time. This effect is even more significant for larger areas; Figure 12 shows partial outflow hydrographs for two simulations of an area 8.5×2.5 m^2. As with the smaller-area simulations, only the vegetated soil hydraulic conductivity was varied to produce these hydrographs, where the parameter spatial distribution was derived and the magnitudes are the same as before. Since vegetated-soil hydraulic conductivity is reduced by grazing but bare-soil conductivity can be left unaffected [8], it is clearly important to simulate interactive infiltration for predicting the hydrologic effects of grazing.

Note that the effective values of ε_2 used for the above simulations are very small, much smaller than the reported typical values [19], and only large enough to control oscillations in

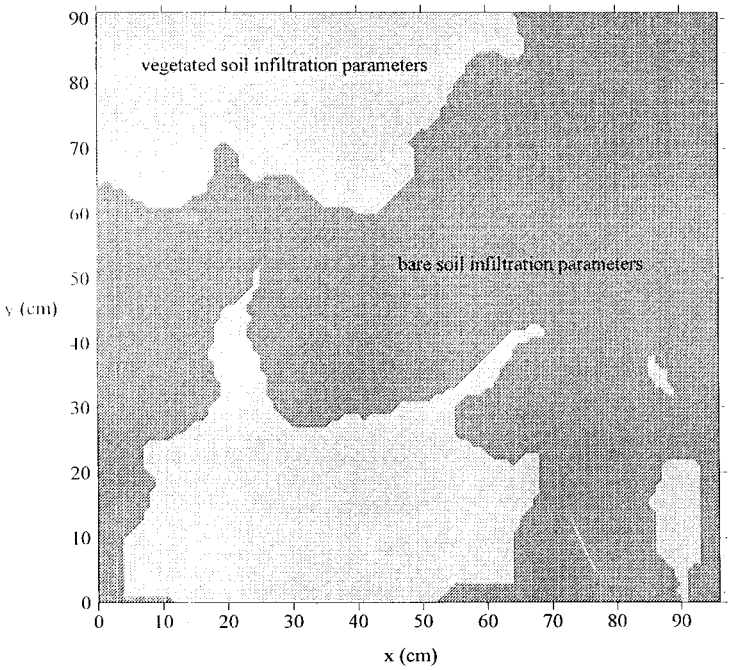

Figure 9. Infiltration parameter spatial distribution.

the vicinity of discontinuities in the flow regime; the upwinded convective acceleration term provides most of the control necessary. Currently, the necessity of the turbulent viscosity term is being evaluated. Preliminary results show that this term is not required for stable solutions of problems with large spatial variability, and its magnitude is generally very small compared with that of the friction slope term. Unrealistically large values of ε_1, though not used here, can greatly affect the velocity field [11].

5. CONCLUSION

A numerical method based on the MacCormack finite difference scheme for simulating discontinuous shallow flow over an infiltrating surface has been developed. Enhancements to the basic scheme include casting it in fractional steps, treating a stiff source term point-implicitly, and upwinding the convective acceleration term. Full dynamic interaction between surface water and infiltration is achieved, where infiltration is modeled with the Green–Ampt equation. It has been shown to be useful for simulating overland flow when spatially variable infiltration and microtopography are important.

With proper attention given to the scale of application (determined by the physical process to be simulated and the degree of spatial variability inherent to that process) such that

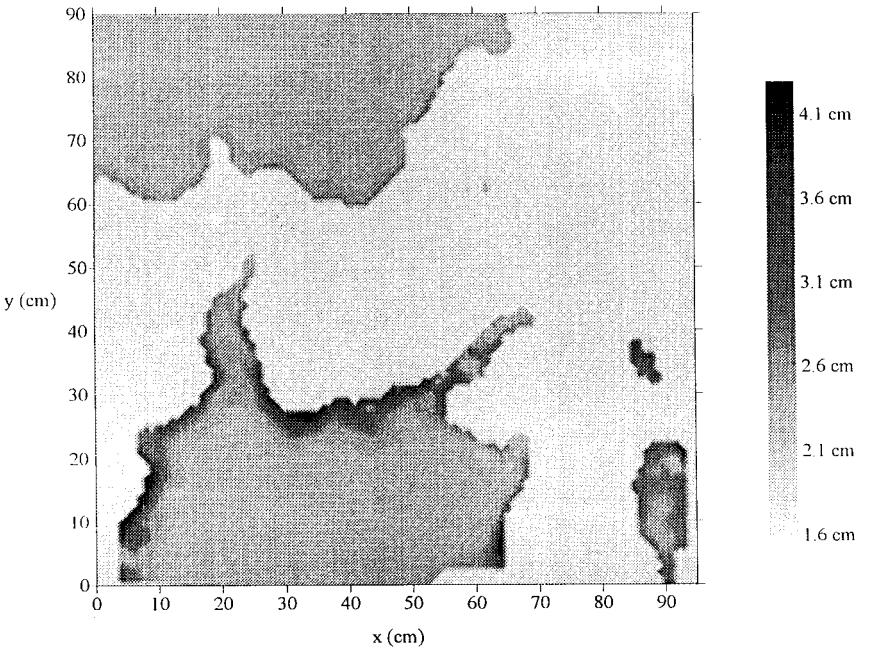

Figure 10. Predicted distribution of cumulative infiltration.

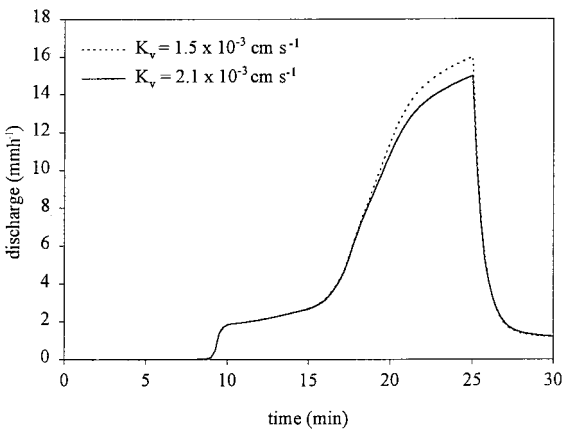

Figure 11. Hydrographs produced with different vegetated-soil hydraulic conductivity distributed as shown in Figure 9.

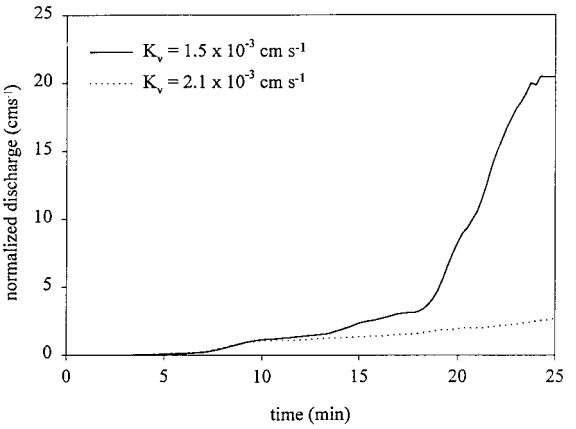

Figure 12. Partial hydrographs for 8.5×2.5 m^2 area produced with different vegetated-soil hydraulic conductivities.

discretization errors are small, the developed method will have several other practical applications. For example, the authors are currently developing a model based on this method to simulate rainfall-driven flash floods, such as the destructive flood that occurred in Fort Collins, Colorado, USA during the summer of 1997. Other potential applications include irrigation, flow in ephemeral stream channels, and tidal flat and wetland circulation.

REFERENCES

1. T. Strelkoff, 'One-dimensional equations of open-channel flow', *J. Hydraul. Div.* ASCE, **95**, 861–876 (1969).
2. W. Zhang and T.W. Cundy, 'Modeling of two-dimensional overland flow', *Water Resour. Res.*, **25**, 2019–2035 (1989).
3. C.B. Vreugdenhil, *Numerical Methods for Shallow-Water Flow*, Kluwer Academic Publishers, Dordrecht, 1994.
4. W.W. Emmett, 'The hydraulics of overland flow on hillslopes', *US Geological Survey Professional Paper 662-A*, 1970.
5. D.A. Woolhiser, 'Simulation of unsteady overland flow', in K. Mahmood and V. Yevjevich (eds.), *Unsteady Flow in Open Channels*, Vol. 2, Water Resources Publications, Fort Collins, CO, 1975, pp. 485–508.
6. E. Playan, 'Two-dimensional hydrodynamic simulation of basin irrigation: analysis of shape effects on irrigation performance', *Ph.D. Dissertation*, Utah State University, 1992.
7. R.W. MacCormack, 'The effect of viscosity in hypervelocity impact cratering', *AIAA Paper 69-354*, Cincinnati, OH, 1969.
8. F.R. Fiedler, 'Hydrodynamic simulation of overland flow with spatially variable infiltration and microtopography', *Ph.D. Dissertation*, Colorado State University, 1997.
9. J.S. Antunes do Carmo, F.J. Seabra Santos and A.B. Almeida, 'Numerical solution of the generalized Serre Equations with the MacCormack finite difference scheme', *Int. J. Numer. Methods Fluids*, **16**, 725–738 (1993).
10. P. Garcia-Navarro and J.M. Saviron, 'MacCormack's method for the numerical simulation of one-dimensional discontinuous open channel flow', *J. Hydraul. Res.*, **30**, 95–105 (1992).
11. R. Garcia and R.A. Kahawita, 'Numerical solution of the St. Venant equations with the MacCormack finite-difference scheme', *Int. J. Numer. Methods Fluids*, **6**, 259–274 (1986).
12. J.A. Liggett and D.A. Woolhiser, 'Finite-difference solutions of the shallow water equations', *Proc. ASCE J. Mech. Div.*, **93**, 39–71 (1967).
13. R.J. LeVeque, *Numerical Methods for Conservation Laws*, Birkhauser, Berlin, 1990.

14. T.R.A. Bussing and E.M. Murman, 'Finite volume method for the calculation of compressible chemically reacting flows', *AIAA J.*, **26**, 1070–1078 (1987).
15. J.A. Liggett, 'Governing equations for free surface flows', in M.H. Chaudhry and L.W. Mays (eds.), *Computer Modeling of Free-Surface and Pressurized Flows*, Kluwer Academic Publishers, Dordrecht, 1994, pp. 3–32.
16. M.B. Abbott and D.R. Basco, *Computational Fluid Dynamics: An Introduction for Engineers*, Longman Scientific & Technical, Essex, UK, 1989.
17. D.R. Basco, 'Computation of rapidly varied unsteady free surface flow', *US Geological Survey*, *Water Resources Investigations Report 83-4284*, 1987.
18. A.W. Jameson, W. Schmidt and E. Turkel, 'Numerical solutions of the Euler equations by finite volume methods using Runge–Kutta time stepping schemes', *AIAA Paper 81-1259*, 1981.
19. R.J. Fennema and M.H. Chaudhry, 'Explicit numerical schemes for unsteady free-surface flows with shocks', *Water Resour. Res.*, **22**, 1923–1930 (1986).
20. W.H. Green and G.A. Ampt, 'Studies on soil physics. Part I. The flow of air and water through soils', *J. Agric. Sci.*, **4**, 1–24 (1911).
21. V.T. Chow, D.R. Maidment and L.W. Mays, *Applied Hydrology*, McGraw-Hill, New York, 1988.
22. R.L. Burden and J.D. Faires, *Numerical Analysis*, PWS_KENT Publishing Company, Boston, MA, 1989.
23. D.A. Woolhiser, R.E. Smith and J.-V. Giraldez, 'Effects of spatial variability of saturated hydraulic conductivity on Hortonian overland flow', *Water Resour. Res.*, **32**, 671–678 (1996).
24. M.A. Kasser and F. Ali, 'The stiff conservation laws and the MacCormack finite difference scheme', *Comput. Methods Appl. Math. Eng.*, **106**, 395–405 (1993).
25. A.K. Jha, J. Akiyama and M. Ura, 'First- and second-order flux difference schemes for dam break problem', *J. Hydraul. Eng.*, **121**, 877–884 (1995).
26. Y. Iwagaki, 'Fundamental studies on the runoff analysis by characteristics', *Disaster Prevention Research Institute Bulletin No. 10*, Kyoto University, Kyoto, Japan, 1955.
27. D.K. Borah, S.N. Prassas and C.V. Alonso, 'Kinematic wave routing incorporating shock fitting', *Water Resour. Res.*, **16**, 529–541 (1980).
28. R.E. Smith and J.-Y. Parlange, 'A parameter-efficient hydrologic infiltration model', *Water Resour. Res.*, **14**, 533–538 (1978).
29. D.R. Maidment, *Handbook of Hydrology*, McGraw-Hill, New York, 1993.

